Novel 2,3-Dihydro-1,4-Benzoxazines as Potent and Orally Bioavailable Inhibitors of Tumor-Driven Angiogenesis[||]

Daniel S. La,*[,†] Julie Belzile,[†] James V. Bready,[‡] Angela Coxon,[‡] Thomas DeMelfi,[‡] Nicholas Doerr,[‡] Juan Estrada,[‡] Julie C. Flynn,[⊥] Shaun R. Flynn,[#] Russell F. Graceffa,[†] Shawn P. Harriman,[⊥] Jay F. Larrow,[†] Alexander M. Long,[§] Matthew W. Martin,[†] Michael J. Morrison,[#] Vinod F. Patel,[†] Philip M. Roveto,[†] Ling Wang,[‡] Matthew M. Weiss,[†] Douglas A. Whittington,[§] Yohannes Teffera,[⊥] Zhiyang Zhao,[⊥] Anthony J. Polverino,[‡] and Jean-Christophe Harmange[†]

Amgen Inc. Chemistry Research and Discovery, Cambridge, Massachusetts 02139, and Thousand Oaks, California 91320

Received September 11, 2007

Angiogenesis is vital for solid tumor growth, and its prevention is a proven strategy for the treatment of disease states such as cancer. The vascular endothelial growth factor (VEGF) pathway provides several opportunities by which small molecules can act as inhibitors of endothelial proliferation and migration. Critical to these processes is signaling through VEGFR-2 or the kinase insert domain receptor (KDR) upon stimulation by its ligand VEGF. Herein, we report the discovery of 2,3-dihydro-1,4-benzoxazines as inhibitors of intrinsic KDR activity ($IC_{50} < 0.1\ \mu M$) and human umbilical vein endothelial cell (HUVEC) proliferation with $IC_{50} < 0.1\ \mu M$. More specifically, compound **16** was identified as a potent (KDR: < 1 nM and HUVEC: 4 nM) and selective inhibitor that exhibited efficacy in angiogenic in vivo models. In addition, this series of molecules is typically well-absorbed orally, further demonstrating the 2,3-dihydro-1,4-benzoxazine moiety as a promising platform for generating kinase-based antiangiogenic therapeutic agents.

Introduction

Excessive or abnormal angiogenesis has been linked to several diseases including cancer, psoriasis, arthritis, endometriosis, and diabetic retinopathy.[1] In a cancer setting, a solid tumor that develops to the size of 2–3 mm in diameter exceeds the limits of passive diffusion for the purposes of acquiring nutrients and disposing of metabolic wastes.[2] Accordingly, tumor progression is reliant on the sprouting and maturation of new blood vessels. Critical to this process is the production of VEGF[a] in response to hypoxia or several upstream activators such as oncogenes, cytokines, or cell growth factors.[3,4] VEGF binds to VEGFR-2 (KDR), a receptor tyrosine kinase (RTK), which upon dimerization/activation by VEGF undergoes autophosphorylation and initiates downstream signaling, ultimately leading to angiogenesis, tumor survival, and tumor migration.

The inhibition of the VEGF pathway has received much attention recently,[5] as evidenced by the recent activity in late stage clinical trials.[6] Most notable with respect to validation of the antiangiogenesis concept is the VEGF monoclonal antibody bevacizumab,[7,8] which has received U.S. Food and Drug Administration approval. Among the small-molecule inhibitors are 1-(4-chloroanilino)-4-(4-pyridylmethyl)phthalazine (PTK787/ZK222584, vatalanib),[9,10] *N*-(4-bromo-2-fluorophenyl)-6-methoxy-7-[(1-methylpiperidin-4-yl)methoxy]quinazolin-4-amine (ZD6474, vandetanib),[11,12] and 3-(4-bromo-2,6-difluoro-benzyloxy)-5-[3-(4-pyrrolidin-1-ylbutyl)ureido]isothiazole-4-carboxylic acid amide (CP547,632)[13] in late stage clinical trials and *N*-[2-(diethylamino)ethyl]-5-[(*Z*)-(5-fluoro-1,2-dihydro-2-oxo-3*H*-indol-3-ylidine)methyl]-2,4-dimethyl-1*H*-pyrrole-3-carboxamide (SU11248, sunitinib)[14–16] and 4-[4-[3-[4-chloro-3-(trifluoromethyl)phenyl]ureido]phenoxy]-*N*-methylpyridine-2-carboxamide (BAY 43-9006, sorafenib),[17] which were approved for the treatment of renal and/or gastrointestinal cancer. Similarly, our program has been focused on the development of small-molecule inhibitors of RTKs, namely, KDR. Our initial efforts resulted in the development of *N*-(2,3-dihydro-3,3-dimethyl-1*H*-indol-6-yl)-2-[(4-pyridinylmethyl)amino]-3-pyridinecarboxamide (AMG 706, motesanib), a highly selective, oral agent that is being evaluated in clinical trials for its ability to inhibit angiogenesis by targeting VEGF receptors 1, 2, and 3, platelet-derived growth factor receptor (PDGFR), and stem cell factor receptor (Kit), which may also confer direct antitumor activity.[18,19]

We have recently identified a series of naphthylamide analogues,[20] shown in Figure 1A, as effective inhibitors of KDR at the enzyme and cellular levels. From X-ray cocrystal analysis, several interactions became apparent and guided our design of subsequent inhibitors. As depicted in Figure 2, compound **1** (VEGFR-2 kinase $IC_{50} = 0.03$ nM and VEGF-HUVEC $IC_{50} =$ 8 nM) binds to the ATP active site of the KDR protein in the inactive, "DFG-out" conformation.[21] The amide functional group participates in hydrogen bond contacts with Glu885 and Asp1046, allowing the aryl chloride to reside in the extended hydrophobic pocket. The naphthalene moiety engages the ATP-binding cleft through van der Waals contacts, and the dimethoxyquinoline interacts with the "hinge region" backbone NH of Cys 919 through a critical hydrogen bond. The high degree of hydrophobic interactions that ligand **1** makes with the protein may provide a rationale for the exquisite potency observed.

Consequently, the average calculated log *P* (cLogP)[22] was greater than 5 for arylamides without solubilizing substituents (Figure 1) presenting solubility issues. In fact, for compound

[||] The PDB codes for cocrystals of compounds **1** and **16** within in the KDR ATP-binding pocket are 3B8Q and 2RL5, respectively.

* To whom correspondence should be addressed. Phone: 617-444-5187. Fax: 617-621-3908. E-mail: daniel.la@amgen.com.

[†] Department of Chemistry Research and Discovery.

[‡] Department of Oncology.

[⊥] Department of Pharmacokinetics and Drug Metabolism.

[#] Department of HTS and Molecular Pharmacology.

[§] Department of Molecular Structure.

[a] Abbreviations: VEGF, vascular endothelial growth factor; KDR, kinase insert domain receptor; HUVEC, human umbilical vein endothelial cell; RTK, receptor tyrosine kinase; PDGFR, platelet-derived growth factor receptor; HTRF, homogenous time-resolved fluorescence.

10.1021/jm701129j CCC: $40.75
Published on Web 02/27/2008

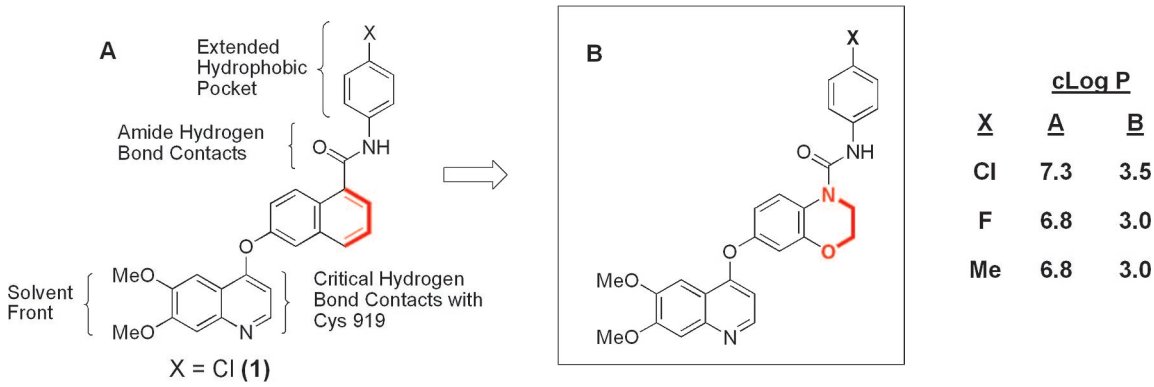

cLog P		
X	A	B
Cl	7.3	3.5
F	6.8	3.0
Me	6.8	3.0

Figure 1. Structural and cLogP analysis of the naphthylamide and 2,3-dihydro-1,4-benzoxazine scaffolds.

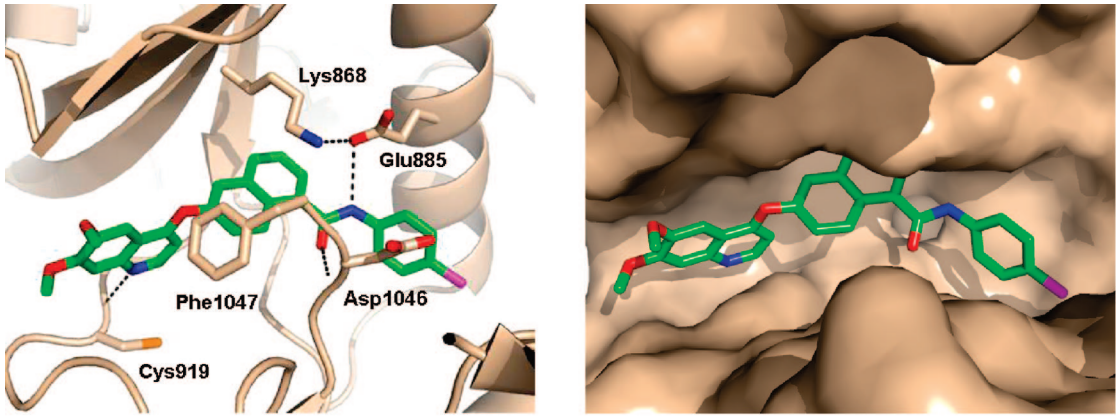

Figure 2. Cocrystal of compound **1** within in the ATP-binding pocket of KDR (PDB code 3B8Q). Key hydrogen bond contacts are shown (dotted lines). In the right diagram, portions of the DFG sequence are omitted for clarity.

1, the solubility was 1.1, <1, and 1.4 μg/mL as measured in 0.01 N HCl, PBS, and SIF, respectively. In addition, the naphthalene core presented potential bioactivation liabilities that could lead to an undesired toxicological profile. These characteristics prompted the design of 2,3-dihydro-1,4-benzoxazines (Figure 1B) that retain the shape and contact elements with the protein while incorporating polar, heteroatom functional groups to improve solubility. Within this chemical series, the cLogP values were approximately 4 calculated log units lower (see Figure 1) than their naphthylamide counterparts. This paper describes the effort leading to the discovery of benzoxazine derivatives as potent, orally available inhibitors of KDR.

Chemistry

Armed with structural information from the naphthylamide series, the principal design features of the 1,4-benzoxazines were rooted in the scaffold's potential to create the appropriate associations with the target enzyme (KDR) while imparting favorable physiochemical properties that would increase success with respect to cell permeability and oral availability. In addition, urea formation as the penultimate bond disconnection enabled rapid analoging, which expedited the generation of in vitro structure–activity relationships (SAR) at the intrinsic, cellular, pharmacokinetic, and toxicology levels.

The synthesis of the benzoxazine analogues began with the amidation/cyclization of aminoresorcinol hydrochloride **2** with chloroacetyl chloride to provide benzoxazinone **3** (Scheme 1). Initial attempts to reduce **3** with $LiAH_4$ and Red-Al failed because of decomposition or complications with product isolation. Borane reduction, however, cleanly provided benzoxazine **4**. This intermediate was then coupled with chloride **5** containing the critical linker or hinge region (on the KDR enzyme) binding moiety. The nucleophilic addition conditions to generate intermediate **6** employed cesium carbonate at elevated temperature to exclusively provide the O-arylated product (Scheme 2). This protocol was applicable to the formation of various biaryl ethers, allowing the investigation and optimization of different linker/hinge region binding groups. The resulting benzoxazine **6** was acylated with isocyanates or *p*-nitrophenyl carbamates to generate the desired urea as KDR inhibitors.

Results and Discussion

Structure–Activity Relationships (SAR). SAR exploration of the 1,4-benzoxazines series was executed with our KDR enzyme inhibition and HUVEC proliferation assays. KDR enzymatic data were obtained utilizing a homogeneous time-resolved fluorescence (HTRF) assay employing a biotinylated gastrin substrate. The enzyme and HUVEC proliferation assays were performed as previously described.[18] Simultaneously, compounds were screened for activity against the cMet, Tie-2, and Lck enzymes as well as cellular FGF driven HUVEC proliferation to provide selectivity information (Table 1). We desired an inhibitor profile free of cMet and Tie-2 activity because their link to tumor angiogenesis would confound our mechanism-based analysis.[23] A selective KDR inhibitor would allow for more accurate target coverage and therefore enable us to reliably account for observed in vivo pharmacology. The Lck kinase was employed as a representative of the Src kinase family, which is involved in critical cellular processes such as cellular growth, differentiation, and signaling.[24]

Initial scanning of substituents placed at the *ortho*, *meta*, and *para* positions on the urea phenyl ring revealed that the meta

Scheme 1. Synthesis of 2,3-Dihydro-1,4-benzoxazines[a]

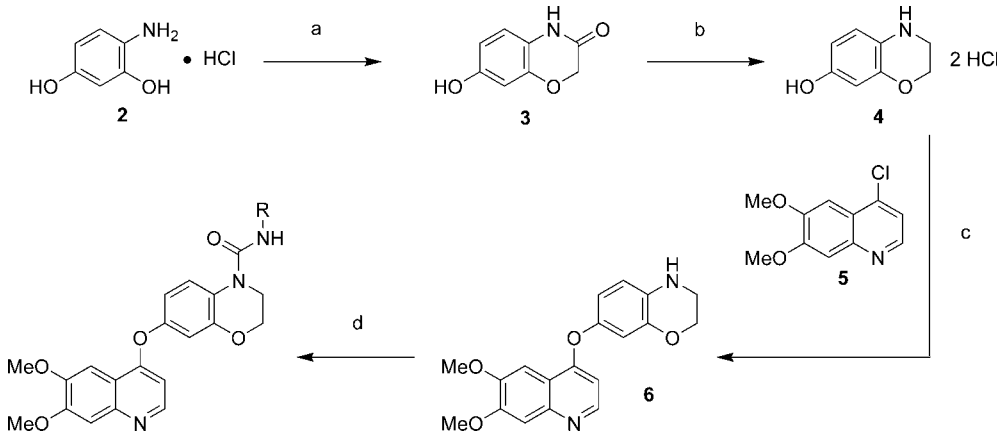

[a] Reagents and conditions: (a) 2-chloroacetyl chloride, Cs_2CO_3, MeCN, 20 °C; (b) BH_3·THF, THF, 20 °C; (c) Cs_2CO_3, 4-chloro-6,7-dimethoxyquinoline (**5**), DMF, 90 °C; (d) RNCO, DCM or R-$NHCO_2$-*p*-nitrophenyl, NEt_3, THF, 50 °C.

Scheme 2. Preparation of Biaryl Ethers[a]

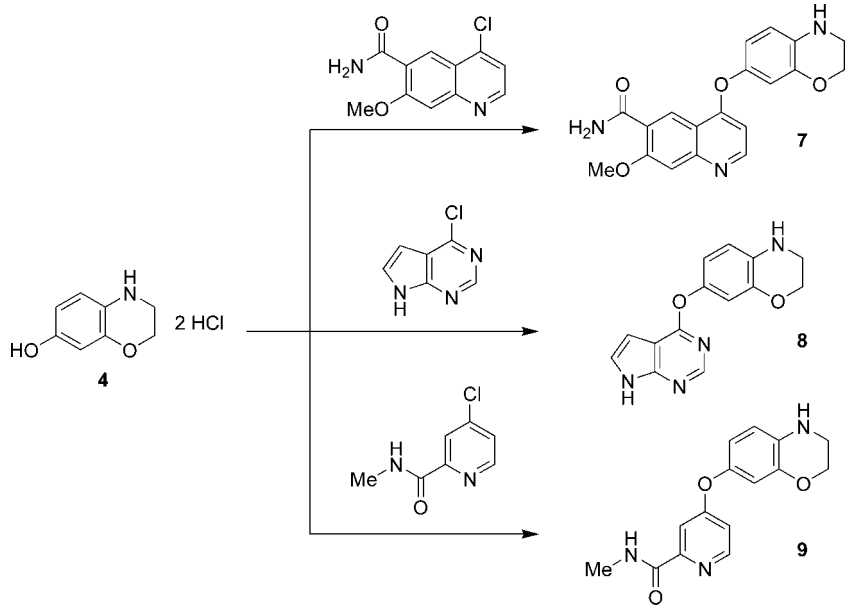

[a] Reagents and conditions: Cs_2CO_3, chlorides **7**, **8**, or **9**, DMF, 90 °C.

and *para* substituted phenyls were optimal for intrinsic and cellular potency. However, para substitution maintained selectivity over the cMet, Tie-2, and Lck as well as FGF-driven HUVEC proliferation (see representative compounds **13** and **16** in Table 1). Substituent at the *ortho* position resulted in reduced cell potency as demonstrated by **11** and **14**. Compounds bearing substitution at the *meta* position were potent in the KDR enzyme and VEGF driven HUVEC proliferation assays but lacked selectivity over Tie-2 and Lck (**12** and **15**).

In an attempt to lower molecular weight, we next turned our attention toward examining alkylureas, starting with small substituents and incrementally increasing in size (see representative compounds **18**–**25**). The smaller compounds were designed to potentially exploit the active "DFG-in" enzyme conformation. It was believed and later confirmed by X-ray crystallography that the arylureas, such as **16**, bind in a "DFG-out" manner (see below) similar to compound **1**. Our preliminary study revealed that an ethylurea was optimal for potency within this series (see compound **20** in Table 1). The ureas **18**, **19** and **21**, on the other hand, were less potent. As exploration expanded to include larger benzylureas, compound **24** proved to be enzymatically and cellularly active. Interestingly, its enantiomer, **25**, was significantly less potent. In general, the alkylureas showed lower potency compared to the arylureas and were therefore not investigated further.

With distinct SAR delineated for the urea moiety, the linker binding portion of the 2,3-dihyro-1,4-benzoxazines was investigated. Three other substructures were studied as exemplified by compounds **26**−**31** (Table 2). The structural design element of these analogues attempted to exploit a possible two-point hydrogen bond contact with Cys 919 as shown in Figure 3. It was thought that the hydrogen bond acceptor of the inhibitor would engage the amide NH of the cysteine residue. Accordingly, the acidic NH or aryl CH of the compound could enhance interaction through hydrogen bonding with the cysteine carbonyl.[25]

The linker binding substituents were evaluated by constructing the *p*-chloro- and *p*-methylarylureas of each structural motif. Carboxamide analogues **26** and **27** were promising, given their enzyme and cell potency in addition to the selectivity over the cMet, Tie-2, Lck and the FGF pathway. The pyrrolopyrimidines

Table 1. Structure–Activity Relationships of the Urea Moiety[a]

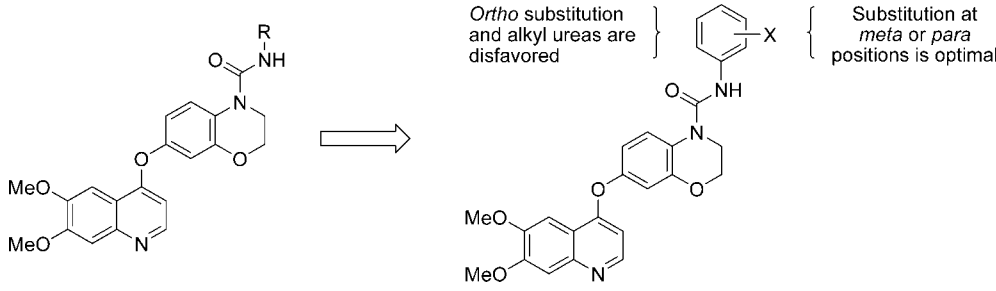

		IC$_{50}$ (nM)					
compd	R	KDR	HUVEC (VEGF)	HUVEC (FGF)	cMet	Tie-2	Lck
10	Ph	1	0.6	340	650	386	188
11	2-Me-Ph	1	45	910	410	1600	27
12	3-Me-Ph	1	0.6	190	350	1	1
13	4-Me-Ph	0.2	3	280	370	1000	63
14	2-Cl-Ph	19	73	230	290	2200	2200
15	3-Cl-Ph	1	0.4	220	230	9	4
16	4-Cl-Ph	0.5	4	1100	300	110	20
17	4-F-Ph	3	2	300	1100	1500	90
18	H	58	280	1100	>4000	>4000	>4000
19	Me	40	100	370	>4000	>4000	2400
20	Et	1	23	780	1400	>4000	1500
21	^{i}Pr	40	52	1100	1200	>4000	1000
22	Bn	53	237	>1100	1600	>4000	500
23	4-Me-Bn	26	360	1100	500	1500	150
24	(*S*)-αMe-Bn	1	3	300	460	260	18
25	(*R*)-αMe-Bn	40	250	1100	210	>4000	78

[a] All kinases were tested at their apparent K_m of ATP with respect to 1 μM peptide substrate. IC$_{50}$ values are the mean of two or more separate determinations in duplicate.

Table 2. Structure–Activity Relationships of the Linker Binding Moiety[a]

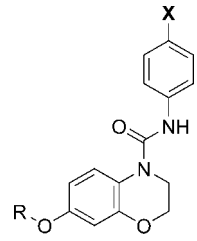

			IC$_{50}$ (nM)					
Compound	R	X	KDR	HUVEC (VEGF)	HUVEC (FGF)	cMet	Tie-2	Lck
16	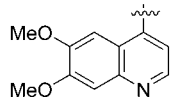	Cl	0.5	4	>1000	300	110	20
13		Me	0.2	3	280	370	1000	63
26	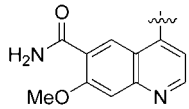	Cl	0.6	1	290	160	290	21
27		Me	0.5	1	300	260	430	19
28	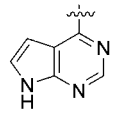	Cl	77	230	>1000	>4000	>4000	>4000
29		Me	26	230	>1000	>4000	>4000	>4000
30	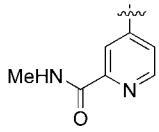	Cl	95	>1000	>1000	>4000	>4000	>4000
31		Me	62	>1000	>1000	>4000	>4000	>4000

[a] All kinases were tested at their apparent K_m of ATP with respect to 1 μM peptide substrate. IC$_{50}$ values are the mean of two or more separate determinations in duplicate.

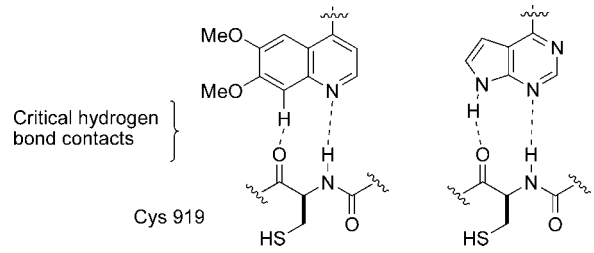

Figure 3. Hydrogen bond interaction between inhibitor and linker/hinge region.

Table 3. Solubility Comparison between Naphthylamides (**A**) and Benzoxazines (**B**)

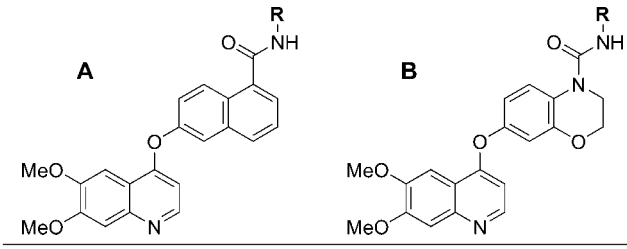

	R	0.01 N HCl	PBS	SIF	cLogP	cLogD$_{6.5}$
A	4-Me-Ph	>200	<1	9.4	6.8	6.7
B (**13**)	4-Me-Ph	>200	<1	22	3.0	2.9
A	3-Cl-Ph	9.5	<1	36	7.3	7.2
B (**15**)	3-Cl-Ph	120	<1	28	3.5	3.4
A	4-Cl-Ph	1.1	<1	1.4	7.3	7.2
B (**16**)	4-Cl-Ph	28	<1	33	3.5	3.4
A	4-F-Ph	67	<1	1.3	6.8	6.7
B (**17**)	4-F-Ph	>200	3.3	41	3.0	2.9
A	Me	>200	1.4	3.0	4.6	4.5
B (**19**)	Me	>200	46	130	1.2	1.1
A	^{i}Pr	>200	<1	5.6	5.4	5.3
B (**21**)	^{i}Pr	>200	3.0	14	2.1	2.0

28 and **29** and *N*-methylpicolinamides **30** and **31**, however, were less potent and not further pursued.

The solubility of the benzoxazine and their naphthylamide predecessors was examined in order to test the hypothesis of introducing heteroatoms to the molecular scaffold to enhance aqueous solubility (see Figure 1). It was believed that proper placement of polar substituents would serve to lower log *P* and that introduction of the sp^3 hybridized ethyl bridge would reduce the planarity of the central rings and limit the potential for π-stacking. By use of an equilibrium solubility method previously described,[26] solubility was determined in three media, 0.01 N HCl, PBS (pH 7), and SIF. In all cases where head-to-head comparisons could be made, the benzoxazines proved to be more soluble. As shown in Table 3, representative benzoxazines containing aromatic and aliphatic ureas possessed greater solubility than their naphthylamide counterparts.

Pharmacokinetic Profiles. On the basis of their desired in vitro cellular potency (<10 nM) and selectivity, several compounds were selected for metabolic stability and pharmacokinetic analysis. This set of compounds displayed good to moderate in vitro stability in human and rat liver microsomal preparations, with the exception of the benzylurea **24** (see Table 4). There was a high correlation between in vitro RLM turnover and in vivo rat iv Cl. Thus, the poor in vitro stability upon incubation with both HLM and RLM was consistent with higher clearance observed after intravenous administration (CL = 0.98 (L/h)/kg). Similarly, compounds **10**, **13**, **17**, and **27** exhibited higher clearance than the *p*-chlorourea analogues **16** and **26**. The moderate clearance of the *p*-methylurea analogues **13** and **27** explains the lower exposure after oral dosing ($AUC_{0\text{-inf}}$ = 1.3 and 0.65 μg h/mL, respectively) in comparison to the *p*-chlorourea analogues **16** and **26** ($AUC_{0\text{-inf}}$ = 7.9 and 4.5 μg h/mL, respectively). However, compounds **16** and **17** exhibited the most stability in HLM and possessed excellent oral bioavailability in rats. Half-lives of compounds in Table 4 ranged from 2 to 6 h in rats with low volume of distribution, which we hypothesized boded well for restricting distribution to predominantly the blood compartment. The protein binding of **16** was similar across species (human, dog, rat, and mouse) and ranged from 99.2% to 99.6%. Because of superior microsomal stability, low clearance, and excellent oral bioavailability (F = 95%), compound **16** was advanced to selectivity assessment against a broad panel of kinases and to determination of pharmacodynamic efficacy.

Selectivity. Compound **16** was evaluated for activity against a broader panel of kinases in order to understand its full target profile. This effort revealed that **16** was selective over a variety of kinases depicted by the heat map illustrated in Figure 4 (green most potent, red least potent). Within the protein tyrosine kinase (PTK) group, **16** was highly selective (>30 fold) over representatives from the Src, Abl, Tie/Tck, FGFR, Tec, and hepatocyte growth factor families. Similarly, selectivity was observed over kinases outside the PTK group (CMGC and AGC), namely, kinases from the MAP, CDK, and RSK families. Not surprisingly, compound **16** was less selective over kinases within the PDGFR family presumably because of significant catalytic domain homology to KDR.

Pharmacodynamic Efficacy. Compound **16** was next examined for in vivo efficacy in a vascular permeability assay and a rat corneal angiogenesis model. These assays were performed as previously described. For the vascular permeability assay[27] HEK 293 cells overexpressing murine VEGF were injected subcutaneously into the abdomen of nude mice. Approximately 22 h later, a single dose of the inhibitor or vehicle was orally administered, and after an additional 6 h, the mice received an iv injection of 0.1 mL 1% Evans blue dye. The mice were then sacrificed, a 1 cm^2 piece of skin overlaying the cells was harvested, and the extracted Evans blue dye was measured. Figure 5A illustrates the dose dependent inhibition of vascular permeability by compound **16**. A statistically significant reduction in extracted Evans blue dye was detected at doses as low as 3 mg/kg (Table 5). In addition, doses of 10 and 30 mg/kg lowered vascular permeability to vehicle control levels.

In vivo efficacy was further demonstrated with a corneal angiogenesis model employing female Sprague Dawley rats.[28] This model entails insertion of either vehicle or VEGF-soaked disks into a pocket in the corneal stroma of an anesthetized rat. The vehicle or compound **16** was orally administered for 7 days. The corneas were then digitally photographed, and the number of blood vessels intersecting a 2.0 mm perpendicular line at the midpoint of the disk placement distance was measured. Figure 5B illustrates the inhibition of angiogenesis in a linear dose dependent fashion. The ED_{50} was calculated to be 0.16 mg/kg for compound **16**. The associated pharmacokinetic analysis determined the exposure to be 2.8 μM h and the C_{max} to be 0.18 μM.

X-ray Structural Analysis. The cocrystal structure of **16** and the KDR enzyme (see Figure 6 and Supporting Information Table S1) highlights the major ligand−target interactions, which presumably account for the observed potencies of the 1,4-benzoxazine scaffold. The quinoline moiety engages the linker

Table 4. Mean Pharmacokinetic Parameters in Male Sprague Dawley Rats[a]

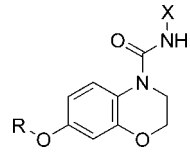

			Metabolic Stability		iv			po			
Compound	R	X	HLM (μL/min/mg)	RLM (μL/min/mg)	CL (L/h/kg)	V_{ss} (L/kg)	$t_{1/2}$ (h)	$AUC_{0\text{-inf}}$ (μg·h/ml)	C_{max} (μg/ml)	T_{max} (h)	F (%)
16		4-Cl-Ph	<14	44	0.24	1.8	6.4	7.9	0.81	3.3	95
10	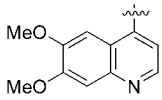	Ph	62	122	1.8	2.1	1.2	ND	ND	ND	ND
13		4-Me-Ph	31	104	0.72	2.8	4.4	1.3	0.30	1.0	47
17		4-F-Ph	17	74	0.82	2.1	3.0	2.6	0.41	2.7	81
24		(*S*)-αMe-Bn	543	188	0.98	1.4	2.3	ND	ND	ND	ND
26	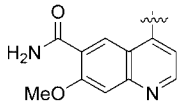	4-Cl-Ph	48	25	0.19	0.50	2.6	4.5	0.82	2.3	46
27		4-Me-Ph	62	96	0.86	1.4	1.6	0.65	0.16	2.3	28

[a] Rats were dosed 0.5 mg/kg iv and 2 mg/kg po.

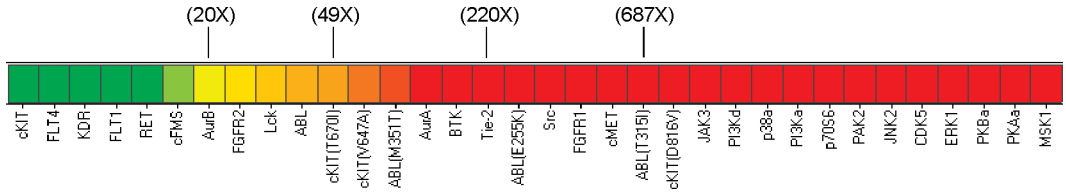

Figure 4. Selectivity heat map for compound **16**.

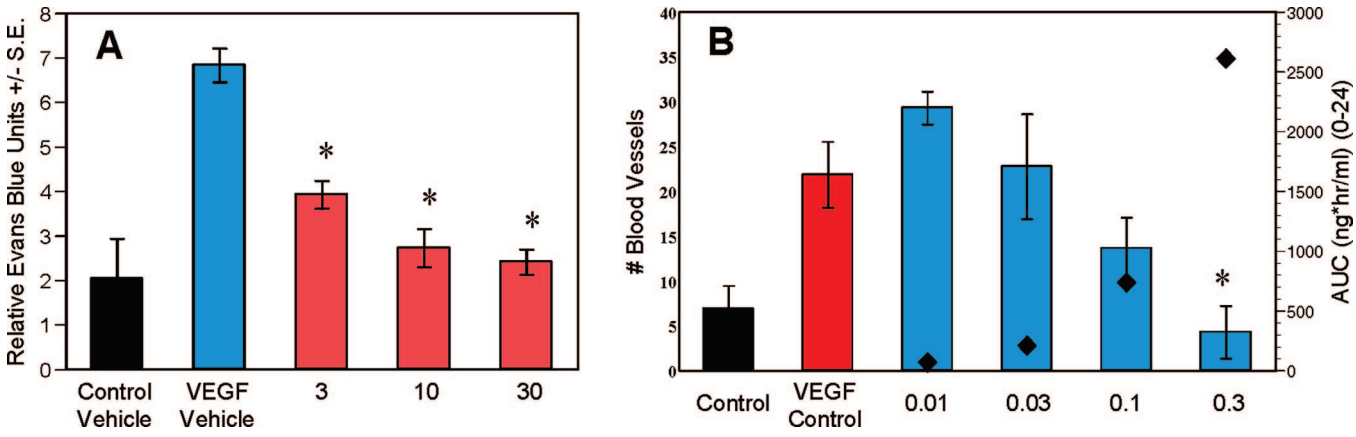

Figure 5. In vivo analysis of compound **16**. (A) Vascular permeability assay. HEK 293 cells transfected with murine VEGF or vector were mixed with Matrigel and injected sc into CD-1 nu/nu mice. A single dose of compound was given, and vascular permeability in the skin overlying the Matrigel plug was assessed 6 h later. Data represent the mean ± standard error ($n = 5$ animals per group): (∗) $P \leq 0.0001$. (B) Rat corneal angiogenesis model. Angiogenesis was induced by implanting a VEGF-soaked or BSA-soaked (control) nylon disk into the corneal stroma. The number of blood vessels intersecting the midpoint between the disk and the limbus was measured after 7 days of dosing vehicle or drug. Data represent the mean ± standard error ($n = 8$ animals per group): (∗) $P = 0.0034$.

region of the enzyme in a 2.9 Å hydrogen bond between the nitrogen and Cys 919. As proposed by the interaction illustrated in Figure 3, an additional hydrogen bond of 3.2 Å is observed through the hydrogen at C8. The experimental electron density mapping shown in Figure 7 illustrates this detailed interaction.[25] The ethereal linkage at the 4-position of the quinoline is sp^2 hybridized (C−O−C angle = 119°) and resides such that the p-orbital lone pair conjugates into the quinoline π-system as opposed to the benzoxazine ring. Across the molecule, two hydrogen bond contacts are observed between the urea carbonyl and Asp 1046 (2.7 Å) and the urea NH and Glu 885 (3.3 Å). In addition, a water molecule serves as a bridge between Lys 868

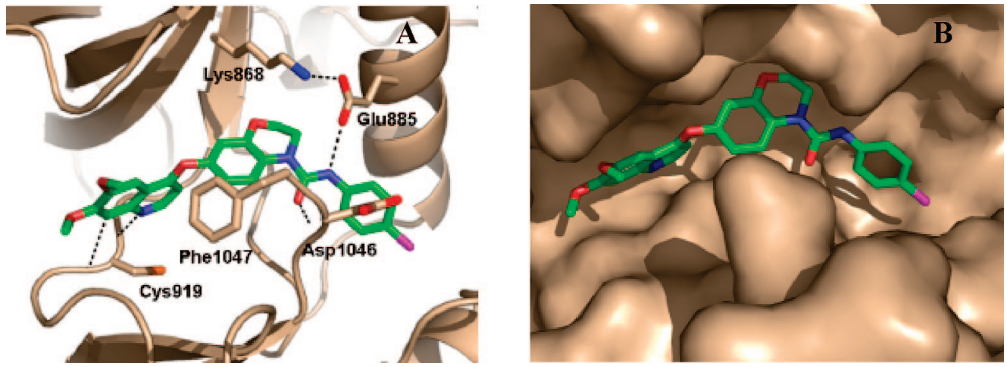

Figure 6. Cocrystal of compound **16** within in the ATP-binding pocket of KDR (PDB code 2RL5). Key hydrogen bond contacts are shown (dotted lines). In part B, portions of the DFG sequence are omitted for clarity.

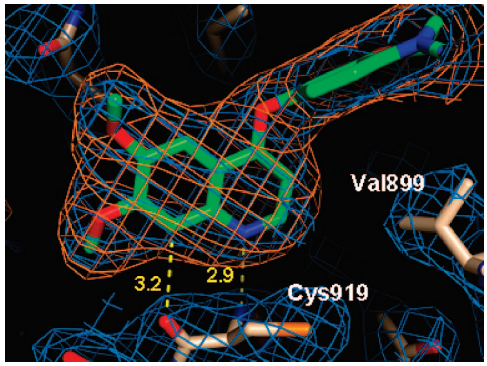

Figure 7. Electron density depicting the interaction of the dimethoxyquinoline ring and Cys919 from the hinge region of KDR. A simulated annealing omit map for the inhibitor (orange, 3σ contour) is superimposed on the final $2F_o - F_c$ map (blue, 1σ contour). Dashed lines indicate hydrogen bonds (distances in angstroms).

Table 5. Pharmacokinetic/Pharmacodynamic Relationship for **16** in the Vascular Permeability and VEGF-Induced Rat Corneal Angiogenesis Models

vascular permeability		rat corneal angiogenesis		
active dose (mg/kg)	exposure at active dose (μM)	ED_{50} (mg/kg)	C_{max} at ED_{50} (μM)	AUC at ED_{50} (μM h)
3	4.6	0.16	0.18	2.8

and Asp 1046 (not shown). Presumably, much of the potency is acquired through van der Waals contacts between the inhibitor and the hydrophobic binding pocket generated upon induced movement of the activation loop by the aryl chloride (compare **16** and **18** of Table 1). Additional van der Waals interactions are seen with the benzoxazine segment and the surrounding lipophilic residues (see Figure 6B).

Conclusions

The novel 2,3-dihydro-1,4-benzoxazine inhibitors and compound **16** in particular have been shown to be effective inhibitors of angiogenesis. This investigation aimed initially to address physical chemical property liabilities of an alternative naphthylamide core, which resulted in the design of the described benzomorpholine series. Our efforts to optimize potency were driven by structural analysis and ultimately revealed several compounds with appropriate levels of activity against KDR and favorable pharmacokinetic properties. This strategy was further validated by in vivo efficacy models, which highlighted the benzoxazines as promising antiangiogenic agents. Further optimization of this series to yield our clinical candidate will be disclosed shortly.

Experimental Section

Unless otherwise noted, all materials were obtained from commercial suppliers and used without further purification. Dry organic solvents (CH_2Cl_2, CH_3CN, DMF, etc.) were purchased from Aldrich packaged under nitrogen in Sure/Seal bottles. Reactions were monitored using an Agilent 1100 series LC−MS instrument with UV detection at 254 nm and a low-resonance electrospray mode (ESI). Medium-pressure liquid chromatography (MPLC) was performed on a CombiFlash Companion (Teledyne Isco) with RediSep normal-phase silica gel (35–60 μm) columns and UV detection at 254 nm. Preparative reversed-phase high-performance liquid chromatography (HPLC) was performed on a Gilson (215 liquid handler), YMC-Pack Pro C18, 150–30 mm i.d. column, eluting with a binary solvent system A and B using a gradient elution (solvent A, H_2O with 0.1% TFA; solvent B, CH_3CN with 0.1% TFA) with UV detection at 254 nm. Purity was measured using Agilent 1100 series HPLC instrument with UV detection at 254 nm (15 min, 1.5 mL/min flow rate; 0−100% 0.1% TFA in CH_3CN/100–0% 0.1% TFA in H_2O). ^{1}H NMR spectra were recorded on a Bruker AV-400 (400 MHz) spectrometer at ambient temperature or on a Varian 400 MHz or Varian 300 MHz spectrometer. Chemical shifts are reported in ppm from the solvent resonance (DMSO-d_6, 2.50 ppm). Data are reported as follows: chemical shift, multiplicity (s = singlet, d = doublet, t = triplet, q = quartet, br = broad, m = multiplet), coupling constants, and number of protons. Mass spectra were obtained on a high-resolution electrospray time-of-flight mass spectrometer. Combustion analysis was performed by Galbraith Laboratories, Inc., Knoxville, TN.

7-Hydroxy-2*H*-benzo[*b*][1,4]oxazin-3(4*H*)-one (3). To a solution of 4-aminoresorcinol hydrochloride (15.0 g, 92.83 mmol) in acetonitrile (300 mL) at 0 °C was added cesium carbonate (90.7 g, 278.4 mmol) followed by a dropwise addition of chloroacetyl chloride (7.76 mL, 97.47 mmol). The reaction mixture was stirred at room temperature for 18 h and then was diluted with absolute ethanol (300 mL). The insoluble materials were filtered and rinsed with absolute ethanol. The filtrate was concentrated under vacuum to afford the crude product as a dark-purple solid. The solid was dissolved in methanol (100 mL), silica was added (100 mL), and the solvent was removed again under vacuum. The solid was loaded onto a pad of silica (800 mL) and eluted with 1:1 ethyl acetate in dichloromethane followed by 100% dichloromethane. After removal of the solvents, the product was obtained as an orange solid (11.71 g, 76%). ^{1}H NMR (DMSO-d_6) δ 9.40 (s, 1H), 8.97–8.95 (m, 1H), 8.72 (s, 1H), 7.99–7.94 (m, 1H), 7.93–7.86 (m, 1H), 7.79 (dd, J = 2.5, 6.8 Hz, 1H), 7.74 (d, J = 9.0 Hz, 1H), 7.64 (s, 1H), 7.50–7.45 (m, 1H), 7.37 (t, J = 9.1 Hz, 1H), 7.02 (d, J = 2.8 Hz, 1H), 6.92 (dd, 9.1, 2.7 Hz, 1H), 6.89–6.86 (m, 1H), 4.37–4.33 (m, 2H), 4.08 (s, 3H), 3.94–3.91 (m, 2H). HRMS [M + H] calcd, 166.049 87; found, 166.050 29.

3,4-Dihydro-2*H*-benzo[*b*][1,4]oxazin-7-ol Hydrochloride (4). A 500 mL round-bottom flask equipped with a magnetic stir bar and a pressure equalizing addition funnel was charged with 7-hydroxy-2*H*-benzo[*b*][1,4]oxazin-3(4*H*)-one (9.74 g, 59 mmol) and anhydrous THF (100 mL) under N_2. The orange-pink mixture was cooled in an ice bath, and borane−THF complex (1 M in THF, 118 mL, 118 mmol, 2 equiv) was added dropwise under a stream of N_2 to remove the H_2 generated. Upon complete addition, the now colorless solution was removed from the ice bath and allowed to warm to ambient temperature. After 3 h of stirring, an aliquot was quenched into MeOH and analyzed by LC−MS, which indicated incomplete consumption of the starting material. After another 3 h of stirring, the reaction was determined to be complete by LC−MS, so the mixture was quenched by the slow addition of MeOH (25 mL) under a stream of N_2. The mixture was then stirred at ambient temperature for 1 h to allow for complete destruction of the borane reagent. The resulting solution was concentrated by rotary evaporation, and the pale-yellow residue was dissolved in MeOH (25 mL). The solution was then cooled in an ice bath under N_2 and a solution of HCl (1 M in Et_2O, 100 mL) was added dropwise, resulting in a white solid suspended in a bright-blue solution. The suspension was aged for 30 min with cooling and then was filtered. The pale-blue solid was washed nearly white with Et_2O/MeOH (4:1, 100 mL) and then was dried under vacuum overnight to yield 3,4-dihydro-2*H*-benzo[*b*][1,4]oxazin-7-ol hydrochloride (10.4 g, 94% yield). ^{1}H NMR (400 MHz, DMSO-d_6) δ 11.22 (br, 1H), 9.85 (br, 1H), 7.07 (d, J = 8.8, 1H), 6.45 (dd, J = 8.7, 2.6, 1H), 6.37 (d, J = 2.5, 1H), 4.32 (m, 2H), 3.48 (m, 2H). HRMS [M + H] calcd, 152.070 60; found, 152.070 60.

7-(6,7-Dimethoxyquinolin-4-yloxy)-3,4-dihydro-2*H*-benzo[*b*][1,4]oxazine (6). A 500 mL three-neck flask equipped with a large magnetic stir bar and a reflux condenser was charged with cesium carbonate (52.46 g, 161 mmol, 3 equiv), 4-chloro-6,7-dimethoxyquinoline (12.00 g, 53.7 mmol, 1.0 equiv), 3,4-dihydro-2*H*-benzo[*b*][1,4]oxazin-7-ol hydrochloride (15.1 g, 80.5 mmol, 1.5 equiv), and DMF (100 mL). The mixture was vacuum-purged (carefully because of CO_2 generation) and then switched to N_2. The brown heterogeneous mixture was then heated to 90–100 °C under N_2 with an oil bath. The reaction was periodically monitored for conversion by LC−MS and showed 75–80% conversion after 3 days. At this point, additional Cs_2CO_3 (8.75 g, 0.5 equiv) and benzomorpholine HCl salt (5.0 g, 0.5 equiv) were added and the mixture was maintained at 100 °C for an additional 26 h until an aliquot indicated about 95% conversion by LC−MS analysis. At this point, the mixture was cooled and then quenched by the addition of water (250 mL). The resulting solid was isolated by vacuum filtration and washed with water. The gray paste was then slurried with MeOH/MTBE (2:1) at ambient temperature, filtered, washed with MeOH, and dried under vacuum to yield 7-(6,7-dimethoxyquinolin-4-yloxy)-3,4-dihydro-2*H*-benzo[*b*][1,4]oxazine (8.84 g, 49%) containing <5% of the chloroquinoline starting material as an off-white solid. The filtrate was concentrated to dryness, reslurried in MeOH, filtered, washed, and dried as before to yield additional material (6.83 g, 38%) containing slightly more chloroquinoline (<5%) as a tan solid. Analytically pure material could be obtained by silica gel chromatography (gradient elution with 0–5% MeOH in dichloromethane). ^{1}H NMR (400 MHz, DMSO-d_6) δ 8.44 (d, J = 5.2, 1H), 7.47 (s, 1H), 7.36 (s, 1H), 6.67–6.65 (m, 1H), 6.60–6.57 (m, 2H), 6.42 (d, J = 5.3, 1H), 5.85 (br, 1H), 4.17–4.15 (m, 2H), 3.93 (s, 3H), 3.92 (s, 3H), 3.32–3.29 (m, 2H). HRMS [M + H] calcd, 339.133 93; found, 339.135 05.

4-(3,4-Dihydro-2*H*-benzo[*b*][1,4]oxazin-7-yloxy)-7-methoxyquinoline-6-carboxamide (7). 4-Chloro-7-methoxyquinoline-6-carboxamide (1.66 g, 7.01 mmol) was added to a sealed round-bottomed vessel followed by 3,4-dihydro-2*H*-benzo[*b*][1,4]oxazin-7-ol (1.59 g, 10.5 mmol) and cesium carbonate (6.86 g, 21.0 mmol). DMF (20 mL) was added, and the vessel was sealed and placed in an oil bath. The resulting mixture was heated to 80 °C and stirred for 16 h. The reaction mixture was then cooled to room temperature, and DMF was removed in vacuo. The crude mixture was purified with silica gel chromotography (5% MeOH in DCM) to provide 2.06 g (83.6%) of product. ^{1}H NMR ($CDCl_3$) δ 9.30 (s, 1H), 8.64 (d, J = 5.3 Hz, 1H), 8.04 (s, 1H), 7.81 (s, 1H), 7.54 (s, 1H), 6.68 (s, 1H), 6.63–6.66 (m, 1H), 6.61 (d, J = 2.5 Hz, 1H), 6.59 (d, J = 2.5 Hz, 1H), 6.53 (d, J = 5.3 Hz, 1H), 4.31 (t, J = 4.3 Hz, 2H), 4.14 (s, 3H), 3.48 (t, J = 4.3 Hz, 2H). HRMS [M + H] calcd, 352.129 18; found, 352.129 62.

7-(7*H*-Pyrrolo[2,3-*d*]pyrimidin-4-yloxy)-3,4-dihydro-2*H*-benzo[*b*][1,4]oxazine (8). A resealable tube was charged with 4-chloro-7*H*-pyrrolo[2,3-*d*]pyrimidine (0.500 g, 3.26 mmol), 3,4-dihydro-2*H*-benzo[*b*][1,4]oxazin-7-ol (0.738 g, 4.88 mmol), cesium carbonate (3.18 g, 9.77 mmol), and DMF (5.0 mL), and the reaction mixture was stirred at 80 °C for 17 h. Additional 3,4-dihydro-2*H*-benzo[*b*][1,4]oxazin-7-ol (0.738 g, 4.88 mmol) and cesium carbonate (3.18 g, 9.77 mmol) were added, and the mixture was stirred at 80 °C for 20 h. The reaction mixture was cooled to room temperature and filtered through a pad of Celite. The filtrate was concentrated, dissolved in DCM/MeOH (∼1:1), filtered through Celite, and concentrated to afford a brown solid. This material was purified twice via column chromatography on silica gel (gradient elution with 0–5% MeOH/DCM) to afford 7-(7*H*-pyrrolo[2,3-*d*]pyrimidin-4-yloxy)-3,4-dihydro-2*H*-benzo[*b*][1,4]oxazine (0.458 g, 1.71 mmol, 52% yield) as an orange solid. ^{1}H NMR (400 MHz, DMSO-d_6) δ ppm 12.12 (s, 1 H), 8.27 (s, 1 H), 7.38–7.41 (m, 1 H), 6.52–6.61 (m, 4 H), 6.29−6.32 (m, 1 H), 4.12–4.17 (m, 2 H), 3.27–3.31 (m, 2 H). HRMS [M + H] calcd, 268.096 03; found, 268.096 03.

4-(3,4-Dihydro-2*H*-benzo[*b*][1,4]oxazin-7-yloxy)-*N*-methylpicolinamide (9). Compound **9** was prepared using the same procedure as compound **7**. ^{1}H NMR (DMSO-d_6) δ 8.75 (s, 1H), 8.46 (d, J = 5.6 Hz, 1H), 7.34 (d, J = 2.7 Hz, 1H), 7.09 (dd, J = 5.6, 2.6 Hz, 1H), 6.59–6.68 (m, 1H), 6.49–6.56 (m, 2H), 5.88 (s, 1H), 4.05–4.24 (m, 2H), 3.26–3.31 (m, 2H), 2.78 (d, J = 4.8 Hz, 3H). HRMS [M + H] calcd, 286.118 62; found, 286.118 75.

7-((6,7-Bis(methyloxy)-4-quinolinyl)oxy)-*N*-phenyl-2,3-dihydro-4*H*-1,4-benzoxazine-4-carboxamide (10). Compound **10** was prepared using the same procedure as compound **16**. ^{1}H NMR (DMSO-d_6) δ 9.13 (s, 1H), 8.50 (d, J = 5.2 Hz, 1H), 7.64 (d, J = 8.8 Hz, 1H), 7.50 (d, J = 8.8 Hz, 1H), 7.48 (s, 1H), 7.39 (s, 1H), 7.29 (dd, J = 7.6, 7.6 Hz, 2H), 7.00 (dd, J = 8.0, 8.0 Hz, 1H), 6.84 (d, J = 2.8 Hz, 1H), 6.78 (dd, J = 8.8, 2.4 Hz, 1H), 6.56 (d, J = 5.2 Hz, 1H), 4.31 (t, J = 4.0 Hz, 2H), 3.94 (s, 3H), 3.93 (s, 3H), 3.90 (t, J = 3.6 Hz, 2H). HPLC purity: 95%. HRMS [M + H] calcd, 458.171 05; found, 458.172 22.

7-((6,7-Bis(methyloxy)-4-quinolinyl)oxy)-*N*-(2-methylphenyl)-2,3-dihydro-4*H*-1,4-benzoxazine-4-carboxamide (11). Compound **11** was prepared using the same procedure as compound **16**. ^{1}H NMR ($CDCl_3$) δ 8.53 (d, J = 5.2 Hz, 1H), 7.84 (d, J = 8.0 Hz, 1H), 7.53 (s, 1H), 7.51 (d, J = 8.8 Hz, 1H), 7.45 (s, 1H), 7.27–7.14 (m, 3H), 7.06 (t, J = 7.2 Hz, 1H), 6.86 (d, J = 2.4 Hz, 1H), 6.82 (dd, J = 8.8, 2.4 Hz, 1H), 6.57 (d, J = 5.2 Hz, 1H), 4.37 (t, J = 4.4 Hz, 2H), 4.06 (s, 6H), 4.01 (t, J = 4.4 Hz, 2H), 2.20 (s, 3H). HRMS [M + H] calcd, 472.186 70; found, 472.187 91. Anal. ($C_{27}H_{25}N_3O_5 \cdot 0.4H_2O$) C, H.

7-((6,7-Bis(methyloxy)-4-quinolinyl)oxy)-*N*-(3-methylphenyl)-2,3-dihydro-4*H*-1,4-benzoxazine-4-carboxamide (12). Compound **12** was prepared using the same procedure as compound **16**. ^{1}H NMR ($CDCl_3$) δ 8.54 (d, J = 5.6 Hz, 1H), 7.52 (s, 1H), 7.44 (s, 1H), 7.43 (d, J = 8.8 Hz, 1H), 7.27–7.17 (m, 4H), 6.92 (d, J = 5.6 Hz, 1H), 6.85 (d, J = 2.4 Hz, 1H), 6.82 (dd, J = 8.8, 2.4 Hz, 1H), 6.61 (d, J = 4.8 Hz, 1H), 4.35 (t, J = 4.4 Hz, 2H), 4.06 (s, 6H), 4.00 (t, J = 4.4 Hz, 2H), 2.35 (s, 3H). HRMS [M + H] calcd, 472.186 70; found, 472.187 11. Anal. ($C_{27}H_{25}N_3O_5$) C, H.

7-((6,7-Bis(methyloxy)-4-quinolinyl)oxy)-*N*-(4-methylphenyl)-2,3-dihydro-4*H*-1,4-benzoxazine-4-carboxamide (13). Compound **13** was prepared using the same procedure as compound **16**. ^{1}H NMR (DMSO-d_6) δ 9.01 (s, 1H), 8.50 (d, J = 5.3 Hz, 1 H), 7.64 (d, J = 8.8 Hz, 1H), 7.48 (s, 1H), 7.39 (s, 2H), 7.37 (s, 1H), 7.10 (d, J = 8.5 Hz, 2H), 6.82 (d, J = 2.8 Hz, 1H), 6.77 (dd, J = 8.9, 2.7 Hz, 1H), 6.56 (d, J = 5.2 Hz, 1H), 4.24 – 4.34 (m, 2H), 3.94 (s, 3H), 3.93 (s, 3H), 3.85–3.91 (m, 2H), 2.25 (s, 3H). HRMS [M

+ H] calcd, 472.186 70; found, 472.187 58. Anal. ($C_{27}H_{25}N_3O_5 \cdot 4.6H_2O$) C, H.

7-((6,7-Bis(methyloxy)-4-quinolinyl)oxy)-*N*-(2-chlorophenyl)-2,3-dihydro-4*H*-1,4-benzoxazine-4-carboxamide (14). Compound **14** was prepared using the same procedure as compound **16**. ^{1}H NMR ($CDCl_3$) δ 8.53 (d, J = 4.8 Hz, 1H), 8.35 (d, J = 8.0 Hz, 1H), 7.98 (s, 1H), 7.54 (d, J = 8.0 Hz, 1H), 7.53 (s, 1H), 7.44 (s, 1H), 7.36–7.27 (m, 2H), 7.02 (t, J = 7.6 Hz, 1H), 6.86–6.84 (m, 2H), 6.57 (d, J = 4.8 Hz, 1H), 4.38 (t, J = 4.0 Hz, 2H), 4.06 (s, 6H), 4.03 (t, J = 4.0 Hz, 2H). HRMS [M + H] calcd, 492.132 07; found, 492.132 36. Anal. ($C_{26}H_{22}ClN_3O_5 \cdot 0.1H_2O$) C, H.

7-((6,7-Bis(methyloxy)-4-quinolinyl)oxy)-*N*-(3-chlorophenyl)-2,3-dihydro-4*H*-1,4-benzoxazine-4-carboxamide (15). Compound **15** was prepared using the same procedure as compound **16**. ^{1}H NMR (DMSO-d_6) δ 9.30 (s, 1H), 8.49 (d, J = 5.2 Hz, 1H), 7.65 (s (br), 1H), 7.61 (d, J = 9.2 Hz, 1H), 7.46 (s, 1H), 7.42 (d, J = 7.2 Hz, 1H), 7.38 (s, 1H), 7.30 (dd, J = 7.6, 7.6 Hz, 1H), 7.04 (d (br), J = 7.6 Hz, 1H), 6.82 (d, J = 2.4 Hz, 1H), 6.77 (dd, J = 8.8, 2.8 Hz, 1H), 6.54 (d, J = 5.2 Hz, 1H), 4.30 (t, J =4.0 Hz, 2H), 3.92 (s, 3H), 3.91 (s, 3H), 3.88 (t, J = 4.0 Hz, 1H). HPLC purity: 98%. HRMS [M + H] calcd, 492.132 07; found, 492.134 04.

***N*-(4-Chlorophenyl)-7-(6,7-dimethoxynaphthalen-1-yloxy)-2,3-dihydrobenzo[*b*][1,4]oxazine-4-carboxamide (16).** To a heterogeneous solution of 1,4-benzoxazine **6** (62.0 mg, 0.183 mmol) in 0.915 mL of anhydrous DCM at room temperature was added 4-chlorophenyl isocyanate (35.2 μL, 0.275 mmol). The resulting solution was stirred at room temperature for 2 h. The crude reaction mixture was then loaded directly onto a MPLC silica gel cartridge. The crude mixture was purified by chromatography (gradient of 100% DCM to 50% DCM/MeOH/NH_4OH (90:10:1)) to yield 48.6 mg of the final desired product (54% yield). ^{1}H NMR (DMSO-d_6) δ 9.16 (s, 1H), 8.40 (d, J = 5.2 Hz, 1H), 7.53 (d, J = 8.8 Hz, 1H), 7.43 (d, J = 8.8 Hz, 1H), 7.37 (s, 1H), 7.29 (s, 1H), 7.25 (d, J = 9.2 Hz, 1H), 6.73 (d, J = 2.8 Hz, 1H), 6.67 (dd, J = 8.8 Hz, 1H), 6.45 (d, J = 5.2 Hz, 1H), 4.21 (t, J = 4.0 Hz, 2H), 3.84 (s, 3H), 3.83 (s, 3H), 3.79 (t, J = 4.4 Hz, 2H). HRMS [M + H] calcd, 492.132 07; found, 492.133 93. Anal. ($C_{26}H_{22}ClN_3O_5 \cdot 0.5H_2O$) C, H.

7-((6,7-Bis(methyloxy)-4-quinolinyl)oxy)-*N*-(4-fluorophenyl)-2,3-dihydro-4*H*-1,4-benzoxazine-4-carboxamide (17). Compound **17** was prepared using the same procedure as compound **16**. ^{1}H NMR (DMSO-d_6) δ 9.14 (s, 1H), 8.50 (d, J = 5.2 Hz, 1H), 7.65 (d, J = 8.8 Hz, 1H), 7.43–7.55 (m, 3H), 7.39 (s, 1H), 7.14 (t, J = 8.9 Hz, 2H), 6.83 (d, J = 2.7 Hz, 1H), 6.78 (dd, J = 8.9, 2.7 Hz, 1H), 6.56 (d, J = 5.2 Hz, 1H), 4.26–4.35 (m, 2H), 3.94 (s, 3H), 3.93 (s, 3H), 3.86–3.92 (m, 2H). HRMS [M + H] calcd, 476.161 63; found, 476.162 11. Anal. ($C_{26}H_{22}FN_3O_5 \cdot 0.6H_2O$) C, H.

7-((6,7-Bis(methyloxy)-4-quinolinyl)oxy)-2,3-dihydro-4*H*-1,4-benzoxazine-4-carboxamide (18). To a solution of 7-(6,7-dimethoxyquinolin-4-yloxy)-3,4-dihydro-2*H*-benzo[*b*][1,4]oxazine (100 mg, 0.296 mmol) in toluene (2 mL) was added trichloroacetyl isocyanate (39.0 μL, 0.325 mmol) at room temperature. The resulting reaction mixture was stirred for 2 h at 60 °C. The solution was cooled to room temperature, and 10% HCl/H_2O (5 mL) was added. The solution was concentrated in vacuo and purified through silica gel chromatography (gradient of 100% CH_2Cl_2 to 30% 90:10:1 CH_2Cl_2/MeOH/NH_4OH) to provide the desired product (29 mg, 25% yield). ^{1}H NMR (DMSO-d_6) δ 8.46 (d, J = 5.13 Hz, 1H), 7.77 (d, J = 8.8 Hz, 1H), 7.46 (s, 1H), 7.37 (s, 1H), 6.67–6.81 (m, 2H), 6.53 (s, 2H), 6.50 (d, J = 5.1 Hz, 1H), 4.21 (t, J = 3.9 Hz, 2H), 3.92 (s, 3H), 3.91 (s, 3H), 3.73 (t, J = 4.0 Hz, 2H). HPLC purity: 97%. HRMS [M + H] calcd, 382.139 75; found, 382.141 11.

7-((6,7-Bis(methyloxy)-4-quinolinyl)oxy)-*N*-methyl-2,3-dihydro-4*H*-1,4-benzoxazine-4-carboxamide (19). Compound **19** was prepared using the same procedure as compound **16**. ^{1}H NMR (DMSO-d_6) δ 8.48 (d, J = 5.0 Hz, 2H), 7.71 (d, J = 9.0 Hz, 1H), 7.47 (s, 1H), 7.39 (s, 1H), 6.88 (q, J = 4.2 Hz, 1H), 6.78 (d, J = 2.8 Hz, 1H), 6.75 (d, J = 8.7 Hz, 1H), 6.53 (d, J = 5.0 Hz, 1H), 4.21 (t, J = 4.3 Hz, 2H), 3.94 (s, 3H), 3.93 (s, 3H), 3.74 (t, J = 4.2 Hz, 2H), 2.68 (d, J = 4.3 Hz, 3H). HRMS [M + H] calcd, 396.155 40; found, 396.157 25. Anal. ($C_{21}H_{21}N_3O_5 \cdot 0.4H_2O$) C, H.

7-((6,7-Bis(methyloxy)-4-quinolinyl)oxy)-*N*-ethyl-2,3-dihydro-4*H*-1,4-benzoxazine-4-carboxamide (20). Compound **20** was prepared using the same procedure as compound **16**. ^{1}H NMR (DMSO-d_6) δ 8.46 (d, J = 5.2 Hz, 1H), 7.68 (d, J = 8.8 Hz, 1H), 7.45 (s, 1H), 7.37 (s, 1H), 6.96 (dd, J = 5.6, 5.6 Hz, 1H), 6.76 (d, J = 2.4 Hz, 1H), 6.73 (dd, J = 8.4, 2.8 Hz, 1H), 6.50 (d, J = 5.6 Hz, 1H), 4.19 (t, J = 4.0 Hz, 2H), 3.92 (s, 3H), 3.90 (s, 3H), 3.72 (t, J = 4.4 Hz, 2H), 3.12 (p, J = 6.4 Hz, 2H), 1.06 (t, J = 7.6 Hz, 3H). HRMS [M + H] calcd, 410.171 05; found, 410.172 38. Anal. ($C_{22}H_{23}N_3O_5 \cdot 0.2H_2O$) C, H.

7-((6,7-Bis(methyloxy)-4-quinolinyl)oxy)-*N*-(1-methylethyl)-2,3-dihydro-4*H*-1,4-benzoxazine-4-carboxamide (21). Compound **21** was prepared using the same procedure as compound **16**. ^{1}H NMR (DMSO-d_6) δ 8.48 (d, J = 5.3 Hz, 1H), 7.71 (d, J = 8.9 Hz, 1H), 7.47 (s, 1H), 7.39 (s, 1H), 6.77 (d, J = 2.9 Hz, 1H), 6.74 (dd, J = 8.9, 2.9 Hz, 1H), 6.69 (d, J = 7.2 Hz, 1H), 6.77 (d, J = 2.9 Hz, 1H), 6.53 (d, J = 5.3 Hz, 1H), 4.22 (t, J = 4.5 Hz, 2H), 3.94 (s, 3H), 3.92 (s, 3H), 3.85–3.83 (m, 1H), 3.73 (t, J = 4.5 Hz, 2H), 1.14 (d, J = 6.5 Hz, 6H). HRMS [M + H] calcd, 424.186 70; found, 424.187 87. Anal. ($C_{23}H_{25}N_3O_5 \cdot 0.2H_2O$) C, H.

7-((6,7-Bis(methyloxy)-4-quinolinyl)oxy)-*N*-(phenylmethyl)-2,3-dihydro-4*H*-1,4-benzoxazine-4-carboxamide (22). Compound **22** was prepared using the same procedure as compound **16**. ^{1}H NMR ($CDCl_3$) δ 8.49 (d, J = 6.2 Hz, 1H), 7.76 (s, 1H), 7.54 (s, 1H), 7.42 (d, J = 8.43 Hz, 1H), 7.29–7.38 (m, 5H), 6.80 (d, J = 2.6 Hz, 1H), 6.73 (dd, J = 8.8, 2.6 Hz, 1H), 6.66 (d, J = 5.5 Hz, 1H), 5.60 (t, J = 5.1 Hz, 1H), 4.53 (d, J = 5.5 Hz, 2H), 4.32 (t, J = 4.13 Hz, 2H), 4.10 (s, 3H), 4.06 (s, 3H), 3.96 (t, J = 4.1 Hz, 2H). HRMS [M + H] calcd, 472.186 70; found, 472.187 79. Anal. ($C_{27}H_{25}N_3O_5 \cdot 1.4H_2O$) C, H.

7-((6,7-Bis(methyloxy)-4-quinolinyl)oxy)-*N*-((4-methylphenyl-)methyl)-2,3-dihydro-4*H*-1,4-benzoxazine-4-carboxamide (23). Compound **23** was prepared using the same procedure as compound **16**. ^{1}H NMR (DMSO-d_6) δ 8.48 (d, J = 5.2 Hz, 1H), 7.72 (d, J = 8.8 Hz, 1H), 7.52 (t, J = 5.8 Hz, 1H), 7.47 (s, 1H), 7.39 (s, 1H), 7.21 (d, J = 8.2 Hz, 2H), 7.13 (d, J = 7.69 Hz, 2H), 6.71–6.83 (m, 1H), 6.52 (d, J = 5.2 Hz, 1H), 5.76 (s, 1H), 4.29 (d, J = 5.5 Hz, 2H), 4.24 (t, J = 4.0 Hz, 2H), 3.94 (s, 3H), 3.92 (s, 3H), 3.80 (t, J = 4.1 Hz, 2H), 2.28 (s, 3H). HRMS [M + H] calcd, 486.202 35; found, 486.203 27. Anal. ($C_{28}H_{27}N_3O_5 \cdot 0.8H_2O$) C, H.

7-((6,7-Bis(methyloxy)-4-quinolinyl)oxy)-*N*-((1*S*)-1-phenylethyl)-2,3-dihydro-4*H*-1,4-benzoxazine-4-carboxamide (24). Compound **24** was prepared using the same procedure as compound **16**. ^{1}H NMR ($CDCl_3$) δ 8.52 (d, J = 5.5 Hz, 1H), 7.51 (s, 1H), 7.44 (s, 1H), 7.27–7.40 (m, 6H), 6.80 (d, J = 2.6 Hz, 1H), 6.75 (dd, J = 8.8, 2.6 Hz, 1H), 6.58 (d, J = 5.5 Hz, 1H), 5.54 (d, J = 7.3 Hz, 1H), 5.10 (dq, J = 7.3, 7.0 Hz, 1H), 4.28 (t, J = 3.7 Hz, 2H), 4.06 (s, 3H), 4.04 (s, 3H), 3.82–4.00 (m, 2H), 1.53 (d, J = 6.97 Hz, 3H). HRMS [M + H] calcd, 486.202 35; found, 486.203 25. Anal. ($C_{28}H_{27}N_3O_5$) C, H.

7-((6,7-Bis(methyloxy)-4-quinolinyl)oxy)-*N*-((1*R*)-1-phenylethyl)-2,3-dihydro-4*H*-1,4-benzoxazine-4-carboxamide (25). Compound **25** was prepared using the same procedure as compound **16**. ^{1}H NMR ($CDCl_3$) δ 8.52 (d, J = 5.5 Hz, 1H), 7.51 (s, 1H), 7.44 (s, 1H), 7.27–7.39 (m, 6H), 6.79 (d, J = 2.57 Hz, 1H), 6.75 (dd, J = 8.62, 2.8 Hz, 1H), 6.58 (d, J = 5.13 Hz, 1H), 5.54 (d, J = 7.7 Hz, 1H), 5.04–5.15 (m, 1H), 4.24–4.30 (m, 2H), 4.06 (s, 3H), 4.04 (s, 3H), 3.83–3.99 (m, 2H), 1.53 (d, J = 6.97 Hz, 3H). HRMS [M + H] calcd, 486.202 35; found, 486.203 19. Anal. ($C_{28}H_{27}N_3O_5 \cdot 0.1H_2O$) C, H.

7-((6-(Aminocarbonyl)-7-(methyloxy)-4-quinolinyl)oxy)-*N*-(4-chlorophenyl)-2,3-dihydro-4*H*-1,4-benzoxazine-4-carboxamide (26). Compound **26** was prepared using the same procedure as compound **16**. Compound **26** was converted to the HCl salt by adding boiling ethanol without completely dissolving the urea. Then 1 N HCl in ethanol was added, and the mixture was slowly cooled to room temperature, with stirring, over 18 h. The solids were collected by filtration and rinsed with ethanol. ^{1}H NMR (DMSO-d_6) δ 9.35 (s, 1H), 8.97 (d, J = 6.3 Hz, 1H), 8.72 (s, 1H), 7.97 (b, 1H), 7.91 (b, 1H), 7.73 (d, J = 8.9 Hz, 1H), 7.67 (s, 1H), 7.57–7.53 (m, 2H), 7.37–7.34 (m, 2H), 7.03 (d, J = 2.7 Hz, 1H), 6.93–6.89

(m, 2H), 4.36–4.33 (m, 2H), 4.08 (s, 3H), 3.94–3.91 (m, 2H). HRMS [M + H] calcd, 505.127 32; found, 505.128 37. Anal. ($C_{26}H_{21}ClN_4O_5 \cdot 1.9H_2O$) C, H.

7-((6-(Aminocarbonyl)-7-(methyloxy)-4-quinolinyl)oxy)-*N*-(4-methylphenyl)-2,3-dihydro-4*H*-1,4-benzoxazine-4-carboxamide (27). Compound **27** was prepared using the same procedure as compound **16**. ^{1}H NMR ($CDCl_3$) δ 9.29 (s, 1H), 8.72 (d, J = 5.1 Hz, 1H), 7.82 (s, 1H), 7.59 (s, 1H), 7.45 (d, J = 8.6 Hz, 1H), 7.33 (d, J = 8.2 Hz, 2H), 7.16 (d, J = 8.7 Hz, 3H), 6.79–6.88 (m, 2H), 6.63 (d, J = 5.3 Hz, 1H), 5.97 (s, 1H), 4.34–4.40 (m, 2H), 4.16 (s, 3H), 3.98–4.05 (m, 2H), 2.34 (s, 3H). HRMS [M + Na] calcd, 507.163 89; found, 507.164 89. Anal. ($C_{27}H_{24}N_4O_5 \cdot 1.2H_2O$) C, H.

***N*-(4-Chlorophenyl)-7-(7*H*-pyrrolo[2,3-*d*]pyrimidin-4-yloxy)-2,3-dihydro-4*H*-1,4-benzoxazine-4-carboxamide (28).** Compound **28** was prepared using the same procedure as compound **16**. ^{1}H NMR (DMSO-d_6) δ 12.20 (s, 1H), 9.29 (s, 1H), 8.31 (s, 1H), 7.48 – 7.63 (m, 3H), 7.42–7.50 (m, 1H), 7.34 (d, J = 8.8 Hz, 2H), 6.82 (d, J = 2.5 Hz, 1H), 6.76 (dd, J = 9.0, 2.5 Hz, 1H), 6.49 (d, J = 1.9 Hz, 1H), 4.30 (s, 2H), 3.89 (s, 2H). HRMS [M + H] calcd, 422.101 44; found, 422.103 07. Anal. ($C_{21}H_{16}ClN_5O_3 \cdot 0.8H_2O$) C, H.

***N*-(4-Methylphenyl)-7-(7*H*-pyrrolo[2,3-*d*]pyrimidin-4-yloxy)-2,3-dihydro-4*H*-1,4-benzoxazine-4-carboxamide (29).** Compound **29** was prepared using the same procedure as compound **16**. ^{1}H NMR (DMSO-d_6) δ 12.20 (s, 1H), 9.04 (s, 1H), 8.31 (s, 1H), 7.56 (d, J = 9.0 Hz, 1H), 7.43–7.49 (m, 1H), 7.38 (d, J = 8.5 Hz, 2H), 7.09 (d, J = 8.3 Hz, 2H), 6.81 (d, J = 2.7 Hz, 1H), 6.75 (dd, J = 8.9, 2.7 Hz, 1H), 6.44–6.51 (m, 1H), 4.22–4.33 (m, 2H), 3.78–3.96 (m, 2H), 2.25 (s, 3H). HRMS [M + H] calcd, 402.156 07; found, 402.157 56. Anal. ($C_{22}H_{19}N_5O_3 \cdot 0.9H_2O$) C, H.

***N*-(4-Chlorophenyl)-7-((2-((methylamino)carbonyl)-4-pyridinyl)oxy)-2,3-dihydro-4*H*-1,4-benzoxazine-4-carboxamide (30).** Compound **30** was prepared using the same procedure as compound **16**. ^{1}H NMR (DMSO-d_6) δ 9.32 (s, 1H), 8.73–8.83 (m, 1H), 8.52 (d, J = 5.6 Hz, 1H), 7.62 (d, J = 9.0 Hz, 1H), 7.53 (d, J = 8.8 Hz, 2H), 7.43 (d, J = 2.4 Hz, 1H), 7.34 (d, J = 8.8 Hz, 2H), 7.19 (dd, J = 5.5, 2.6 Hz, 1H), 6.81 (d, J = 2.7 Hz, 1H), 6.74 (dd, J = 9.0, 2.7 Hz, 1H), 4.31 (s, 2H), 3.9 (s, 2H), 2.79 (d, J = 4.8 Hz, 3H). HRMS [M + H] calcd, 439.116 76; found, 439.117 87. Anal. Calcd for $C_{22}H_{19}ClN_4O_4$: C, 60.21; H, 4.36; N, 12.77. Found: C, 60.55; H, 4.90; N, 11.76.

7-((2-((Methylamino)carbonyl)-4-pyridinyl)oxy)-*N*-(4-methylphenyl)-2,3-dihydro-4*H*-1,4-benzoxazine-4-carboxamide (31). Compound **31** was prepared using the same procedure as compound **16**. ^{1}H NMR (DMSO-d_6) δ 9.08 (s, 1H), 8.73–8.82 (m, 1H), 8.51 (d, J = 5.6 Hz, 1H), 7.62 (d, J = 9.0 Hz, 1H), 7.43 (d, J = 2.5 Hz, 1H), 7.38 (d, J = 8.5 Hz, 2H), 7.18 (dd, J = 5.6, 2.5 Hz, 1H), 7.09 (d, J = 8.3 Hz, 2H), 6.79 (d, J = 2.8 Hz, 1H), 6.73 (dd, J = 8.9, 2.8 Hz, 1H), 4.23–4.34 (m, 2H), 3.81–3.95 (m, 2H), 2.79 (d, J = 4.8 Hz, 3H), 2.25 (s, 3H). HRMS [M + H] calcd, 419.171 38; found, 419.172 44. Anal. ($C_{23}H_{22}N_4O_4$) C, H.

Supporting Information Available: Analytical data for synthesized compounds and data collection and refinement statistics for X-ray structure of compound **16** bound to KDR. This material is available free of charge via the Internet at http://pubs.acs.org.

References

(1) Carmeliet, P. Angiogenesis in Health and Disease. *Nat. Med.* **2003**, *9*, 653–660.

(2) Folkman, J. Tumor Angiogenesis: Therapeutic Implications. *N. Engl. J. Med.* **1971**, *285*, 1182–1186.

(3) Ferrara, N.; Gerber, H.; LeCouter, J. The Biology of VEGF and Its Receptor. *Nat. Med.* **2003**, *9*, 669–676.

(4) Breier, G.; Risau, W. The Role of Vascular Endothelial Growth Factor in Blood Vessel Formation. *Trends Cell Biol.* **1996**, *6*, 454–456.

(5) Boehm, T.; Folkman, J.; Browder, T.; O'Reilly, M. Antiangiogenic Therapy of Experimental Cancer Does Not Induce Acquired Drug Resistance. *Nature* **1997**, *390*, 404–407.

(6) Zakarija, A.; Soff, G. Update on Angiogenesis Inhibitors. *Curr. Opin. Oncol.* **2005**, *17*, 578–583.

(7) D'Adamo, D.; Anderson, S.; Albritton, K.; Yamada, J.; Riedel, E.; Scheu, K.; Schwartz, G.; Chen, H.; Maki, R. Phase II Study of Doxorubicin and Bevacizumab for Patients with Metastatic Soft-Tissue Sarcomas. *J. Clin. Oncol.* **2005**, *23*, 7135–7142.

(8) Yang, J.; Haworth, L.; Sherry, R.; Hwu, P.; Schwartzentruber, D.; Topalian, S.; Steinberg, S.; Chen, H.; Rosenberg, S. A Randomized Trial of Bevacizumab, an Anti-Vascular Endothelial Growth Factor Antibody, for Metastatic Renal Cancer. *N. Engl. J. Med.* **2003**, *349*, 427–434.

(9) Drevs, J.; Müller-Driver, R.; Wittig, C.; Fuxius, S.; Esser, N.; Hugenschmidt, H.; Konerding, M.; Allegrini, P.; Wood, J.; Hennig, J.; Unger, C.; Marmé, D. PTK787/ZK 222584, a Specific Vascular Endothelial Growth Factor-Receptor Tyrosine Kinase Inhibitor, Affects the Anatomy of the Tumor Vascular Bed and the Functional Vascular Properties As Detected by Dynamic Enhanced Magnetic Resonance Imaging. *Cancer Res.* **2002**, *62*, 4015–4022.

(10) Bold, G.; Altman, K.; Frei, J.; Lang, M.; Manley, P.; Traxler, P.; Wietfeld, B.; Brüggen, J.; Buchdunger, E.; Cozens, R.; Ferrari, S.; Furet, P.; Hofmann, F.; Martiny-Baron, G.; Mestan, J.; Rösel, J.; Sills, M.; Stover, D.; Acemoglu, F.; Boss, E.; Emmenegger, R.; Lässer, L.; Masso, E.; Roth, R.; Schlachter, C.; Vetterli, W.; Wyss, D.; Wood, J. New Anilinophthalazines as Potent and Orally Well Absorbed Inhibitors of the VEGF Receptor Tyrosine Kinases Useful as Antagonists of Tumor-Driven Angiogenesis. *J. Med. Chem.* **2000**, *43*, 2310–2323.

(11) Ciardiello, F.; Caputo, R.; Damiano, V.; Caputo, R.; Troiani, T.; Vitagliano, D.; Carlomangno, F.; Veneziani, B.; Fontanini, G.; Bianco, R.; Tortora, G. Antitumor Effects of ZD6474, a Small Molecule Vascular Endothelial Growth Factor Receptor Tyrosine Kinase Inhibitor, with Additional Activity Against Epidermal Growth Factor Receptor Tyrosine Kinase. *Clin. Cancer Res.* **2003**, *9*, 1546–1556.

(12) Hennequin, L.; Stokes, E.; Thomas, A.; Johnstone, C.; Plé, P.; Ogilvie, D.; Dukes, M.; Wedge, S.; Kendrew, J.; Curwen, J. Novel 4-Anilinoquinazolines with C-7 Basic Side Chains: Design and Structure Activity Relationship of a Series of Potent, Orally Active, VEGF Receptor Tyrosine Kinase Inhibitors. *J. Med. Chem.* **2002**, *45*, 1300–1312.

(13) Beebe, J.; Jani, J.; Knauth, E.; Goodwin, P.; Higdon, C.; Rossi, A.; Emerson, E.; Finkelstein, M.; Floyd, E.; Harriman, S.; Atherton, J.; Hillerman, S.; Soderstrom, C.; Kou, K.; Gant, T.; Noe, M.; Foster, B.; Rastinejad, F.; Marx, M.; Schaeffer, T.; Whalen, P.; Roberts, W. Pharmacological Characterization of CP-547,632, a Novel Vascular Endothelial Growth Factor Receptor-2 Tyrosine Kinase Inhibitor for Cancer Therapy. *Cancer Res.* **2003**, *63*, 7301–7309.

(14) Pietras, K.; Hanahan, D. A Multitargeted, Metronomic, and Maximum-Tolerated Dose "Chemo-Switch" Regimen Is Antiangiogenic, Producing Objective Responses and Survival Benefit in a Mouse Model of Cancer. *J. Clin. Oncol.* **2005**, *23*, 939–952.

(15) Mendel, D.; Laird, D.; Xin, X.; Louie, S.; Christensen, J.; Li, G.; Schreck, R.; Abrams, T.; Ngai, T.; Lee, L.; Murray, L.; Carver, J.; Chan, E.; Moss, K.; Haznedar, J.; Sukbuntherng, J.; Blake, R.; Sun, L.; Tang, C.; Miller, T.; Shirazian, S.; McMahon, G.; Cherrington, J. In Vivo Antitumor Activity of SU11248, a Novel Tyrosine Kinase Inhibitor Targeting Vascular Endothelial Growth Factor and Platelet-Derived Growth Factor Receptors: Determination of a Pharmacokinetic/Pharmacodynamic Relationship. *Clin. Cancer Res.* **2003**, *9*, 327–337.

(16) Atkins, M.; Jones, C. A.; Kirkpatrick, P. Sunitinib Maleate. *Nat. Rev. Drug Discovery* **2006**, *5* (4), 279–280.

(17) Ng, R.; Chen, E. X. Sorafinib (BAY 43-9006): Review of Clinical Developement. *Curr. Clin. Pharmacol.* **2006**, *1*, 223–228.

(18) Polverino, A.; Coxon, A.; Starnes, C.; Diaz, Z.; Demelfi, T.; Wang, L.; Bready, J.; Estrada, J.; Cattley, R.; Kaufman, S.; Chen, D.; Gan, Y.; Kumar, G.; Meyer, J.; Neervannan, S.; Alva, G.; Talvenheimo, J.; Montestruque, S.; Tasker, A.; Patel, V.; Radinsky, R.; Kendall, R. AMG 706, an Oral, Multikinase Inhibitor That Selectively Targets Vascular Endothelial Growth Factor, Platelet-Derived Growth Factor, and Kit Receptors, Potently Inhibits Angiogenesis and Induces Regression in Tumor Xenografts. *Cancer Res.* **2006**, *66* (17), 8715–8721.

(19) Rosen, L. S.; Kurzrock, R.; Mulay, M.; Van Vugt, A.; Purdom, M.; Ng, C.; Silverman, J.; Koutsoukos, A.; Sun, Y.-N.; Bass, M. B.; Xu, R. Y.; Polverino, A.; Wiezorek, J. S.; Chang, D. D.; Benjamin, R.; Herbst, R. S. Safety, Pharmacokinetics, and Efficacy of AMG 706, an Oral Multikinase Inhibitor, in Patients with Advanced Solid Tumors. *J. Clin. Oncol.* **2007**, *25* (17), 2369–2376.

(20) (a) Harmange, J.; Weiss, M.; Germain, J.; Polverino, A. J.; Borg, G.; Bready, J.; Buckner, W.; Chen, D.; Choquette, D.; Coxon, A.; DeMelfi, T. DiPietro, L.; Doerr, N.; Estrada, J.; Fellows, I.; Flynn, J.; Graceffa, R. F.; Harriman, S. P.; Kaufman, S.; La, D. S.; Long, A.; Martin, M. W.; Neervannan, S.; Patel, V. F.; Potashman, M.; Regal, K.; Roveto, P. M.; Schrag, M. L.; Starnes, C.; Tasker, A.; Teffera, Y.; Wang, L.; White, R. D.; Whittington, D.; Zanon, R. Naphthamides as Novel and Potent VEGF Receptor Tyrosine Kinase Inhibitors: Design,

Synthesis, and Evaluation. *J. Med. Chem.* **2008**, *51*, 1649–1667. (b) Weiss, M. M.; Harmange, J.; Polverino, A. J.; Bauer, D.; Berry, L.; Berry, V.; Borg, G.; Bready, J.; Bretz, A.; Chen, D.; Chi, V.; Choquette, D.; Coxon, A.; DeMelfi, T.; Doerr, N.; Estrada, J.; Fellows, I.; Flynn, J.; Graceffa, R. F.; Harriman, S. P.; Kaufman, S.; La, D. S.; Long, A.; Neervannan, S.; Patel, V. F.; Potashman, M.; Regal, K.; Roveto, P. M.; Schrag, M. L.; Starnes, C.; Tasker, A.; Teffera, Y.; Whittington, D.; Zanon, R. Evaluation of a Series of Naphthamides as Potent, Orally Active VEGFR-2 Tyrosine Kinase Inhibitors. *J. Med. Chem.* **2008**, *51*, 1668–1680.

(21) Liu, Y.; Gray, N. Rational Design of Inhibitors That Bind to Inactive Kinase Conformations. *Nat. Chem. Biol.* **2006**, *2*, 358–364.

(22) cLogP values were calculated employing software from ACD Labs (Advanced Chemistry Development Inc.).

(23) (a) Mazzone, M.; Comoglio, P. M. The Met Pathway: Master Switch and Drug Target in Cancer Progression. *FASEB J.* **2006**, *20*, 1611–1621. (b) Yu, Q. The Dynamic Roles of Angiopoietins in Tumor Angiogenesis. *Future Med.* **2005**, *1*, 475–484.

(24) (a) Parson, S. J.; Parsons, J. T. Src Family Kinases, Key Regulators of Signal Transduction. *Oncogene* **2004**, *23*, 7906–7909. (b) Palacios, E. H.; Weiss, A. Function of the Src-Family Kinases, Lck and Fyn, in T-Cell Development and Activation. *Oncogene* **2004**, *23*, 7990–8000.

(25) Pierce, A. C.; Sandretto, K. L.; Bemis, G. W. Kinase Inhibitors and the Case for CH−O Hydrogen Bonds in Protein-Ligand Binding. *Proteins: Struct., Funct., Genet.* **2002**, *49* (4), 567–576.

(26) Tan, H.; Semin, D.; Wacker, M.; Cheetham, J. An Automated Screening Assay for Determination of Aqueous Equilibrium Solubility Enabling SPR Study during Drug Lead Optimization. *J. Assoc. Lab. Autom.* **2005**, *10*, 364–373.

(27) Vascular permeability was induced using a modified Miles assay: Miles, A.; Miles, E. Vascular Reactions to Histamine, Histamine-Liberator and Leukotaxine in the Skin of Guinea-Pigs. *J. Physiol.* **1952**, *118*, 228–257.

(28) Coxon, A.; Bolon, B.; Estrada, J.; Kaufman, S.; Scully, S.; Rattan, A.; Duryea, D.; Hu, Y.; Rex, K.; Pacheco, E.; Van, G.; Zack, D.; Feige, U. Inhibition of Interleukin-1 but Not Tumor Necrosis Factor Suppresses Neovascularization in Rat Models of Corneal Angiogenesis and Adjuvant Arthritis. *Arthritis Rheum.* **2002**, *46*, 2604–2612.

JM701129J